J. Meas. Sci. Instrum., 2025, 16(1): 107-118.
DOI: 10.62756/jmsi.1674-8042.2025011
http://jmsi.publish.founderss.cn/
jmsi@nuc.edu.cn

FPGA-based design of laser gyro signal acquisition circuit

CHEN Jing, LI Jinming*

School of Semiconductors and Physics, North University of China, Taiyuan 030051, China

***Corresponding author:** LI Jinming (lijinming@nuc.edu.cn)

Received: March 16, 2024 **Revised:** July 15, 2024 **Accepted:** October 12, 2024

Abstract: With the continuous evolution of electronic technology, field-programmable gate array (FPGA) has demonstrated significant advantages in the realm of signal acquisition and processing, and signal acquisition plays a pivotal role in the practical applications of laser gyros. By analysis of the output signals from a laser gyro and an accelerometer, this paper presents a circuit design for signal acquisition of the laser gyro based on domestic devices. The design incorporates a finite impulse response (FIR) filter to process the gyro signal and employs a small-volume, impact-resistant quartz flexible accelerometer for signal aquisition. Simulation results demonstrate that the errors in X, Y, and Z axes fall within acceptable ranges while meeting filtering requirements. The use of FPGA for signal acquisition and preprocessing enhances configuration flexibility, which provides an idea and method for optimizing performance and processing signals in laser gyro applications.

Key words: laser gyro; signal acquisition; field-programmable gate array (FPGA); finite impulse response (FIR) filter; accelerometer

0 Introduction

The gyro is a device that detects and maintains direction based on the principle of angular momentum conservation. It provides the angular velocity of the installed carrier and assists in calculating the position, velocity, and attitude of the carrier for inertial navigation systems[1]. In the 1960s, gyros were extensively employed in military, aerospace, and other domains in the United States[2,3]. During the development history of second-generation gyros, laser gyros and fiber optic gyros were introduced. Laser gyros make high-precision measurements via the Sagnac effect within an annular optical path. The Sagnac effect refers to two light beams returning to their starting point after respectively travelling clockwise and counterclockwise along a closed optical path. If there is no rotation within this closed path, both light beams return simultaneously, otherwise, there is a time difference between their returns[4]. This time difference is known as optical path difference which is directly proportional to externally applied angular velocity input. Therefore, by measuring this optical path difference between two light beams, it becomes possible to calculate rotational speed in laser gyros. After extensive development and improvement over time due to its versatility as well as high precision and reliability[5], laser gyro has become one of the primary types used in aviation, aerospace engineering, and navigation systems among other fields[6].

The types of laser gyros developed by various countries mainly include single-axis two-frequency mechanical dithered laser gyros, space triaxial laser gyros, and multioscillator ring laser gyros with four-frequency differentials, etc. [7]. With their superior temperature performance, mechanical properties, and scale factor stability, laser gyros have become the primary choice for navigation-grade and strategic-grade inertial navigation applications[8]. Along with the continuous advancements of integrated circuit design technology and the rapid progress in microelectronics technology, high accuracy has been achieved within the assembly of inertial instruments. However, high-precision acquisition and processing circuits are required for collecting gyro signals and transmitting them to the navigation computer for subsequent data processing and analysis. Therefore, the data acquisition circuit plays a crucial role in facilitating practical applications of laser gyros by providing more reliable technical support.

1 Design of hardware circuit

The field-programmable gate array (FPGA) primarily handles the acquisition and preprocessing of gyro signals, accelerometer data, and external communication. Signal

isolation and analog-digital signal conversion are accomplished through an external circuit. The overall framework diagram of hardware circuit design is shown in Fig.1.

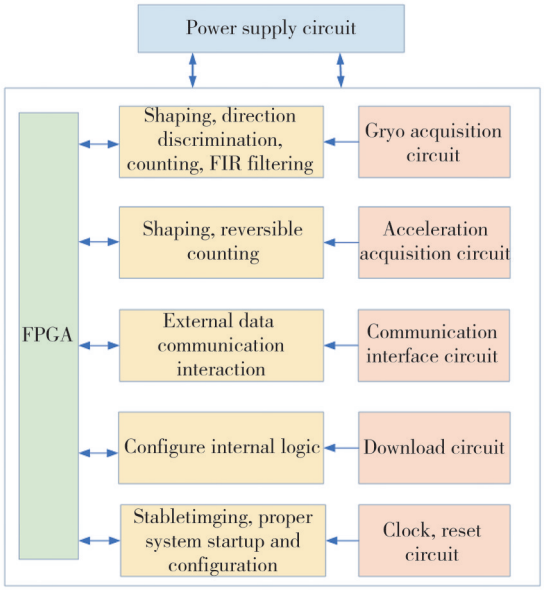

Fig. 1 Overall block diagram of hardware circuit

1.1 Gyro signal isolation circuit

The importance of the gyro signal isolation circuit in the system lies in its role of ensuring the accuracy and stability of the signal acquisition circuit and the overall reliability of system performance. When the laser gyro square wave signal is input to the FPGA, it is necessary to use an isolation circuit to separate the output part from the input part and prevent electrical connection between them[9]. Commonly used electrical isolation methods include electromagnetic coupling and photoelectric coupling[10]. Electromagnetic coupling is often used in industrial high-pressure environments, but large size of devices are not suitable for integrated design of circuit boards. Photoelectric coupling offers several advantages, such as unidirectional signal transmission, complete electrical isolation between the input and the output, no influence of the input signal on the output signal, and strong resistance to common-mode interference[11]. Therefore, photoelectric coupling is chosen. Based on optocoupler technology, the input signal is isolated from the electrical connection by using FPGA system to prevent direct current, thus ensuring the accuracy and stability of signal acquisition. The design utilizes the HCPL-063L photocoupler, operating at 5 V.

This device consists of two pairs of light-emitting diodes and photoreceptors, facilitating the isolation of electro-optical-telecommunication signal conversion. It is commonly employed in isolating line receivers, microprocessor system interfaces, and similar applications[12]. Fig. 2 illustrates the circuit diagram depicting the *Y*-axis gyro signal isolation. The gyro outputs two square waves SIN2_TL and COS3_TL to the photoelectric coupling isolation device while incorporating a transient voltage suppression (TVS) diode at the gyro's input port to prevent damage caused by excessive external voltages. As the output signal level from the photoelectric coupling device does not match that set by the FPGA's I/O pin, a bus transceiver is utilized to convert logic levels from 5 V to 3.3 V.

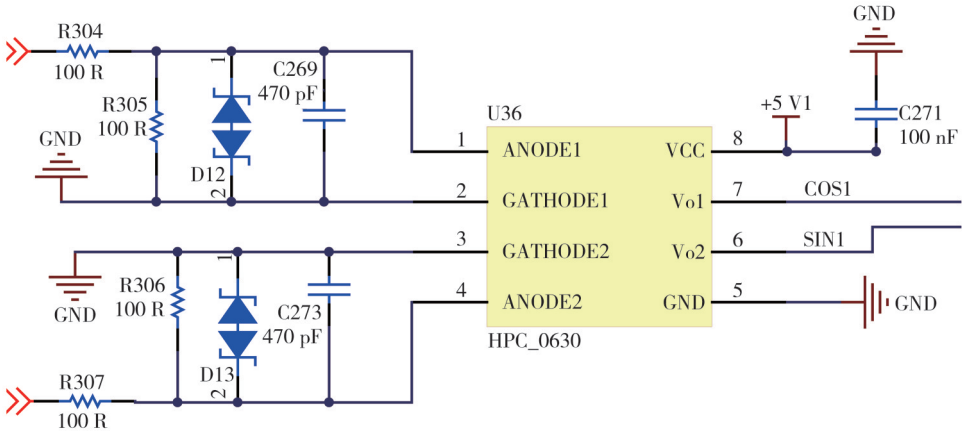

Fig. 2 *Y*-axis gyro signal isolation circuit

1.2 Accelerometer signal acquisition circuit

The output current signal of the quartz flexible accelerometer is directly proportional to the acceleration along its sensitive axis. After undergoing signal conversion, acquisition, and processing, the acceleration in this direction can be accurately determined[13]. Commonly-used schemes for converting accelerometer current signals include I/V and V/F conversion-based aquistion, I/V and A/D conversion-based aquistion, as well as I/F conversion-based aquistion. The I/V and V/F conversion-based

acquisition involves converting the current signal from the accelerometer into a voltage signal. This voltage signal is then transformed into a frequency pulse signal. This method utilizes two consecutive conversions for signal acquisition. However, employing multiple conversions introduces additional circuitry noise interference, thereby reducing sampling accuracy[14]. The I/V and A/D conversion-based aquistion converts the current signal from the accelerometer into a voltage signal, which is subsequently collected by an A/D converter with high-precision and low-temperature operation. Although this approach offers simple circuit design, high precision, and rapid conversion speed, it suffers from imbalanced conversion range capability and poor noise suppression ability[15]. Additionally, I/F conversion-based aquistion performs an integral transformation on the current output of an accelerometer to convert it into a pulse-like waveform that exhibits excellent anti-interference properties while delivering smoother signals. Consequently, this technique has gained widespread adoption in transforming accelerometer signals[16]. In the design, an I/F conversion-based aquistion method is employed, and HMVFC341LT50A3UE-LS02G current frequency conversion circuit manufactured is utilized to convert the current signal output by the accelerometer into a pulse signal. Each conversion circuit incorporates three frequency conversion functions, with power supply voltage requirements of ±15 V and +5 V, as illustrated in Fig.3.

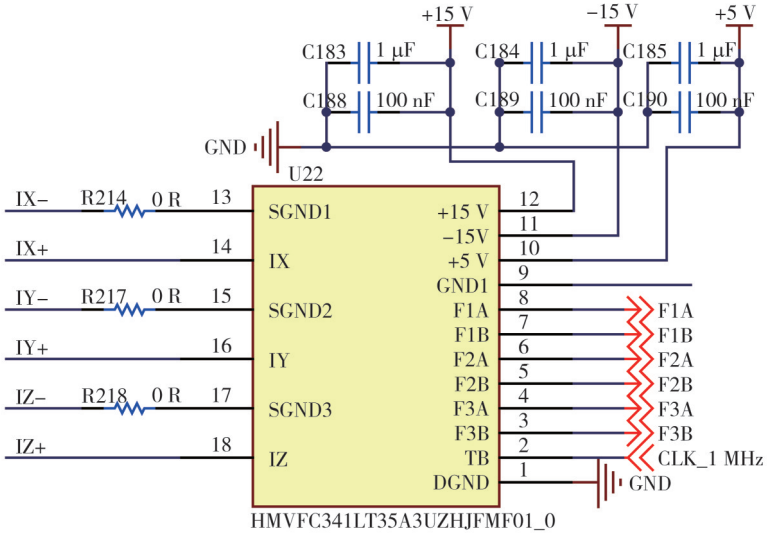

Fig. 3 I/F conversion-based acquisition circuit

The positive terminals of the *X*-, *Y*-, and *Z*-axes accelerometers are connected to pins IX, IY, and IZ, respectively, while the negative terminals are connected to SGND. Pins F1A, F1B, F2A, F2B, F3A, and F3B serve as output pins of the conversion circuit. To minimize interference, the output pulse signal is transmitted to an FPGA for collection through an acceleration signal isolation circuit (as depicted in Fig.4). This isolation circuit utilizes ADI's ADuM1200 dual-channel digital isolator to provide a complete electrical isolation between input and output. The power pins VDD1 and VDD2 are independently powered to support a maximum data rate of 25 Mbps for level conversion.

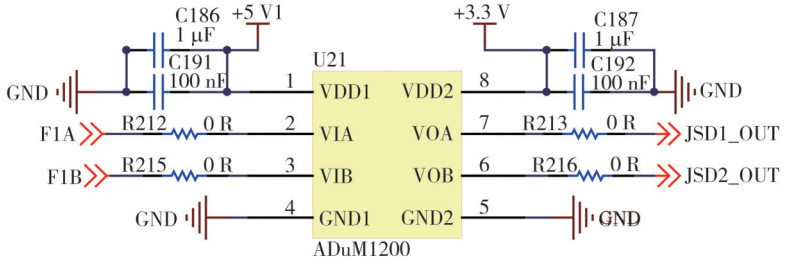

Fig. 4 Acceleration signal isolation circuit

2 Acquisition and filtering of gyro signal

Laser gyros are high-precision devices that operate on the principle of the Sagnac effect in a ring optical path. The Sagnac effect refers to the phenomenon where two light beams propagate clockwise (CW) and counterclockwise

(CCW) respectively in a closed optical loop and return to the emission point. When the closed optical path is stationary, both light beams arrive at the transmitting point simultaneously. However, if the closed optical path rotates, there will be an unequal time taken for the two light beams to return due to their different propagation distances. This discrepancy is known as optical path difference and is directly proportional to the external input angular speed. Therefore, by measuring this optical path difference between the two beams of light, we can determine information about the rotational speed of the laser gyro. The Sagnac effect principle is illustrated in Fig.5.

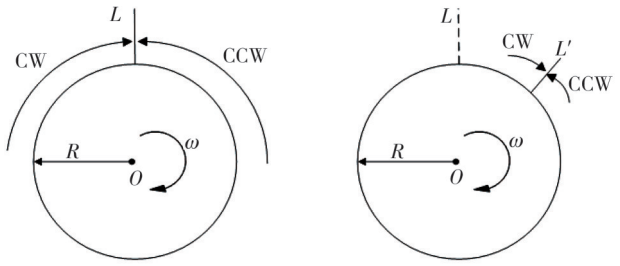

(a) Closed optical path(static) (b) Closed optical path(rotatory)

Fig. 5 Sagnac effect diagram

When the closed optical path remains unrotated, both light beams can simultaneously reach point L, with the time taken as

$$t=\frac{2\pi R}{c}, \tag{1}$$

where c represents the speed of light, and R denotes the radius of the resonant cavity within the closed optical path. When the closed optical path undergoes rotation at an angular velocity ω, the time for two light beams to reach the intersection point L' during rotation is ascertained by

$$\begin{cases} t_{\mathrm{CW}}=\dfrac{2\pi R+R\omega t_{\mathrm{CW}}}{c}, \\ t_{\mathrm{CCW}}=\dfrac{2\pi R-R\omega t_{\mathrm{CCW}}}{c}, \end{cases} \tag{2}$$

where t_{cw} represents the time for the fair-clock propagation to reach the transmitting point, t_{ccw} represents the time for the optical backclock propagation to reach the transmitting point, and ω denotes the angular velocity of rotation of the closed optical path. The time difference and optical path difference of the two beams are

$$\begin{cases} \Delta t=t_{\mathrm{CW}}-t_{\mathrm{CCW}}=\dfrac{4\pi R^2\omega}{c^2}, \\ \Delta L=L_{\mathrm{CW}}-L_{\mathrm{CCW}}=\dfrac{4S\omega}{c}, \end{cases} \tag{3}$$

where S represents the enclosed area of the optical path, Δt represents the time difference experienced by light traveling in the forward and backward directions, ΔL represents the disparity in the optical path length for light propagating in these respective directions, while ω signifies the angular velocity of the resonant cavity's rotation. However, due to the rapid speed of light propagation, the volume of the laser gyro constrains the radius of the closed optical circuit, making accurate measurement of optical path difference ΔL challenging. The circuit can measure the optical frequency difference signal, which is directly proportional to the rotation angular velocity of the gyro. The resonant frequencies v_{CW} and v_{CCW} are designed for two light beams respectively, and when satisfying resonant condition $q=\dfrac{L}{\lambda}$, Eq. (4) can be derived as

$$\begin{cases} v_{\mathrm{CW}}=\dfrac{c}{\lambda}=\dfrac{qc}{L_{\mathrm{CW}}}, \\ v_{\mathrm{CCW}}=\dfrac{c}{\lambda}=\dfrac{qc}{L_{\mathrm{CCW}}}, \end{cases} \tag{4}$$

where v_{CW} and v_{CCW} denote the resonant frequency of light clockwise and counterclockwise, respectively; c is the speed of light, λ denotes the wavelength of laser light in the resonant cavity, q denotes the resonance quality factor; and L_{cw} and L_{ccw} denote clockwise and counterclockwise paths of optical propagation in the resonator.

The optical frequency difference is derived from the discrepancy in resonant frequencies of the two beams and is expressed by

$$\Delta v=\frac{4S}{\lambda L}\omega, \tag{5}$$

where Δv is proportional to the angular velocity ω of the resonant cavity, and $\dfrac{4S}{\lambda L}$ represents the calibration factor of the laser gyro. Given that angular velocity $\omega=\dfrac{\Delta\theta}{\Delta t}$, the number of pulses obtained through integration over time t can be calculated by

$$N=\int_0^t \Delta v\,\mathrm{d}t=\frac{4S}{\lambda L}\int_0^t \omega\,\mathrm{d}t=\frac{4S}{\lambda L}\Delta\theta, \tag{6}$$

where $\Delta\theta$ is the rotational angular velocity of the laser gyro in t time. Therefore, as long as the collection, phase discrimination, and filtering of laser gyro signal are completed, the angular velocity of the carrier can be obtained.

The laser gyro outputs two pulse signals: SIN represents sinusoidal pulse signal, and COS represents cosine pulse signal. When the laser gyro rotates clockwise, the SIN signal output phase exceeds the COS signal phase by 90°, and when the laser gyro rotates counterclockwise, the SIN signal output phase lags behind the COS signal phase by 90°. By analyzing these phase differences, the direction of carrier rotation can be determined. Moreover, a reversible

counter is employed to accumulate input pulses and calculate the angular velocity of carrier rotation[17]. Fig.6 shows the overall design of the gyro signal acquisition and filtering module.

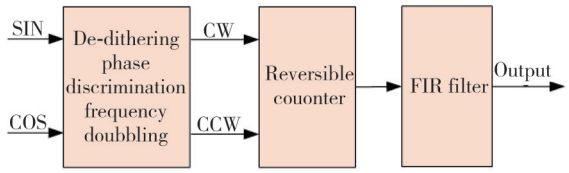

Fig. 6 Overall design of gyro signal acquisition and filtering module

2.1 Gyro signal acquisition module

In the practical circuit, due to external electromagnetic interference, the signal is susceptible to dither during level conversion, resulting in missampling. Therefore, it is necessary to employ software-based de-dithering techniques to enhance sampling accuracy. The clock frequency of the module is set at 120 MHz, which significantly exceeds that of the input signal from the gyro signal acquisition module. This enables effective signal sampling. For level conversion of the input signal, if it remains stable within N clock cycles, it is regarded as a valid signal; otherwise, any level changes caused by external interference are disregarded as false triggers. To maintain phase alignment between the two input signals and ensure accurate measurement, a delay of 5 cycles is simultaneously implemented. After completing the process of signal dithering, the determination of laser gyro rotation direction relies on analyzing phase changes in the input SIN and COS signals, as depicted in Fig.7. In this figure, SIN and COS represent two pulse signals. In contrast, CW represents forward rotation-generated pulse signals and CCW represents reverse rotation-generated pulse signals. The frequency of CW and CCW pulse signals is quadruple that of SIN and COS pulse signals. These CW and CCW pulse signals are counted using a reversible counter for further analysis. When there is a leading phase difference of 90° between SIN and COS signals, the quadrupling frequency can be achieved through the generation of CW pulse signals while their values are accumulated by a reversible counter accordingly. Similarly, when there is a leading phase difference of 90° between COS and SIN signals, the generation of CCW pulse signals also achieves quadrupling frequency with corresponding decremental counting performed by a reversible counter.

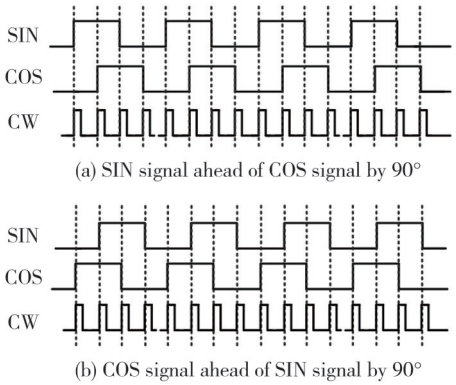

Fig. 7 Gyro signal phase identification

This paper presents a simulation file designed to model the input of a gyro pulse signal, followed by a simulation test conducted with Modelsim software. The resulting simulation waveform is depicted in Fig.8.

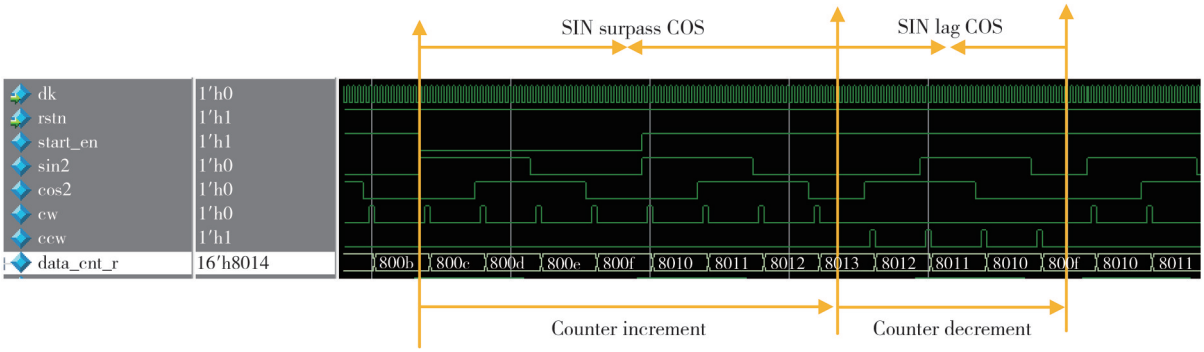

Fig. 8 Simulation diagram of gyro acquisition module

In Fig.8, when the SIN signal leads the COS signal, the CW signal enables frequency quadrupling and facilitates accumulation through a reversible counter. Conversely, when the SIN signal lags behind the COS signal, the CCW signal also achieves quadrupling of frequency while enabling decrement functionality through a reversible counter.

2.2 Gyro signal filtering module

The introduction of lasers has significantly advanced the practical application of the Sagnac effect, although it can also induce lock-in effect. Due to laser medium dispersion, mode competition, and other factors, when the frequencies of the clockwise and counterclockwise

traveling waves approach a certain proximity, they experience mutual coupling. This results in frequency locking, where both frequencies become identical, eliminating deviation and leading to a zero beat frequency output from the gyro[18].

$$\Delta v=\begin{cases}K\omega\sqrt{1-\dfrac{\omega_{\mathrm{L}}^2}{\omega^2}}, & |\omega|>\omega_{\mathrm{L}},\\ 0, & |\omega|\leqslant\omega_{\mathrm{L}}.\end{cases}\tag{7}$$

Ideally, the laser gyro frequency difference Δv should be linearly correlated with the carrier speed Ω, and the gyro has no output only when the speed is zero. Nevertheless, the output of the actual laser gyro is depicted in Fig. 9(b), where the gyro already has no output when the carrier rotational speed is low (but not zero). This phenomenon is particularly evident in two-frequency gyros with low rotational speed[19]. In large two-frequency gyros, the intrinsic rotation of the earth can assist the gyro in breaking through the locking region, and thus the lock-in effect is an impediment that must be overcome by small, especially miniature, laser gyros. The dither bias method is widely employed to address the lock-in effect on account of its straightforward design and low cost. In the production process of the gyro, the lock-in effect is typically eliminated by applying a sinusoidal waveform of a certain frequency[20]. Currently, for the dither bias laser gyro, the whole cycle counting method is mainly utilized for demodulation. Although it can effectively eliminate the bias signals, it is incapable of effectively eliminating the random dither signals concealed in the dither bias laser gyro and the noise resulting from other factors. To precisely obtain the effective input rate of the gyro, digital filtering technology must be applied at its output.

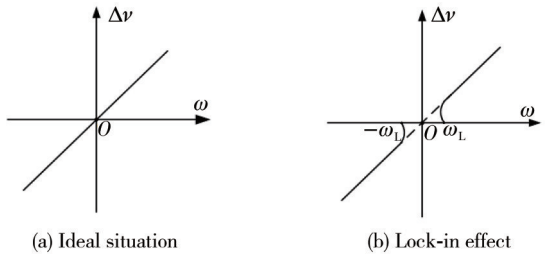

(a) Ideal situation (b) Lock-in effect

Fig. 9 Output curve of laser gyro

Common digital filtering methods encompass finite impulse response (FIR) filters, infinite impulse response (IIR) filters, and IIR notch filters. Among them, the IIR filter can achieve greater stopband attenuation with a lower order and has a mature formula for reference. However, its input and output do not possess linear phase characteristics, which might lead to frequency dispersion. The IIR notch filter can attenuate the dither signal in the laser gyro output signal by setting the frequency of the dither signal as its center frequency with a lower order. Nevertheless, the frequency of the dither signal is not fixed, thus dynamically adjusting the center frequency of the filter adds complexity to the design. Additionally, since it still adopts the IIR approach, the passband suffers from the disadvantage of nonlinear phase response[21]. In contrast, FIR filters are typically effective in eliminating dither and random noise signals while fulfilling the amplitude-frequency characteristics of the system and providing strictly linear phase characteristics. FIR filters only have zeros and poles at $Z=0$, ensuring the stability of the system[22]. Therefore, it is a more appropriate option to employ FIR filters for filtering in the design. FPGAs, with their well-structured internal logic arrays and abundant connectivity resources, are particularly suitable for digital signal processing tasks, enhancing the speed of computation, reducing the latency of data sampling, and increasing the parallelism and portability of the design while lowering the cost.

An FIR filter consists of a finite number of sampled values which convert convolution sums into summations at each sampling moment[23]. The input signal to the filter and its corresponding output can be calculated by

$$y[n]=x[n]*f[n]=\sum_{k=0}^{N-1}x[k]f[n-k],\tag{8}$$

where N denotes the order of the FIR filter, and $x[k]$ represents the sampled value of the FIR filter at tap moment k. The tap coefficients of the FIR filter are denoted by $f[n-k]$, $0\leqslant k\leqslant N\text{-}1$, $k\in\mathbf{N}^+$. The output of the FIR filter is expressed as a linear convolution of the input sequence $x[n]$ and the unit impulse response $f(n)$.

The FIR filter is characterized by its order N, the sampling value $x[k]$ at time k, and the tap coefficient $f[n-k]$. The sampling frequency of the FIR filter is set to 10 kHz, with a passband frequency range of 0 Hz—300 Hz and a cut-off frequency of 500 Hz. The filter has an order of 128.

The 50 Hz sinusoidal signal emulates the angular velocity change signal of the laser gyro, while the 600 Hz sinusoidal signal simulates the mechanical dithered signal of the laser gyro. Random white Gaussian noise is incorporated to simulate external interference. The generated signal is depicted in Fig.10. By superimposing these three signals, the collected gyro signal is fed into an FIR filter, and the waveforms of the output signal, filtered signal, and target signal are displayed. As illustrated in Fig. 11, there is consistency between the filtered and target signals' waveforms. To determine any change in frequency within

the input signals, a frequency spectrum analysis is conducted on both the superimposed and filtered signals, as shown in Fig.12. It can be intuitively seen that the signal frequency of the superimposed signal is mainly 50 Hz and 600 Hz. The filtered frequency is 50 Hz, 600 Hz can be filtered out, and the FIR filter configuration and filtering coefficient are correct and the filtering function can be realized.

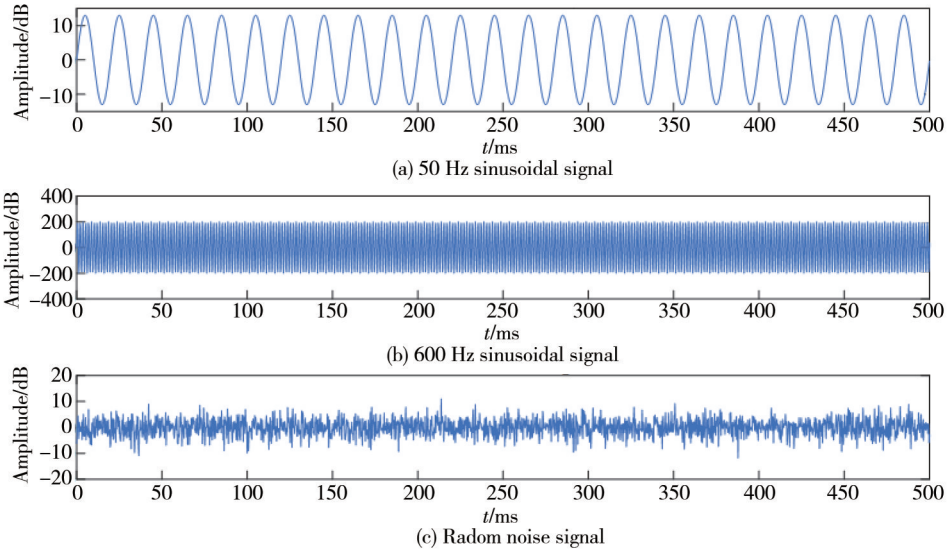

Fig. 10 Simulated input of vibration signal for laser gyro

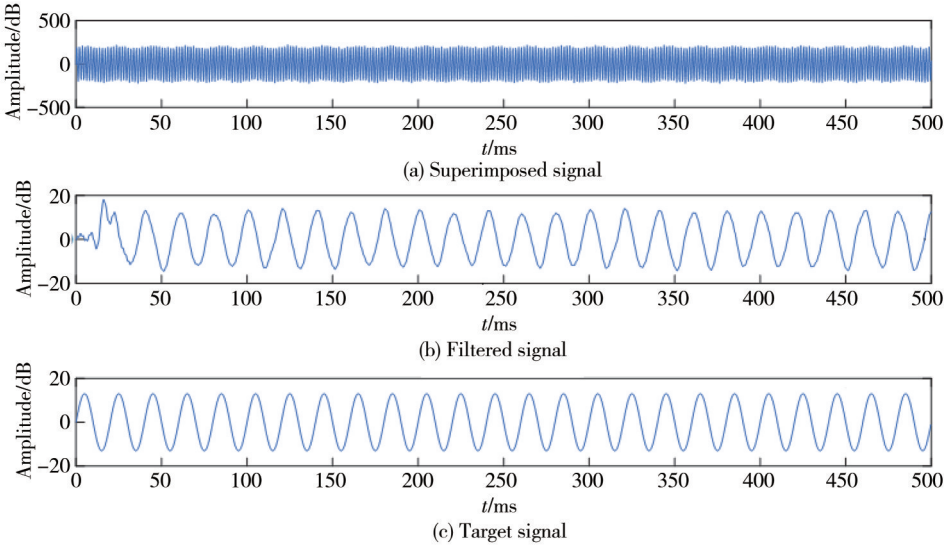

Fig. 11 Waveform display of gyro acquisition signal and filtered signal

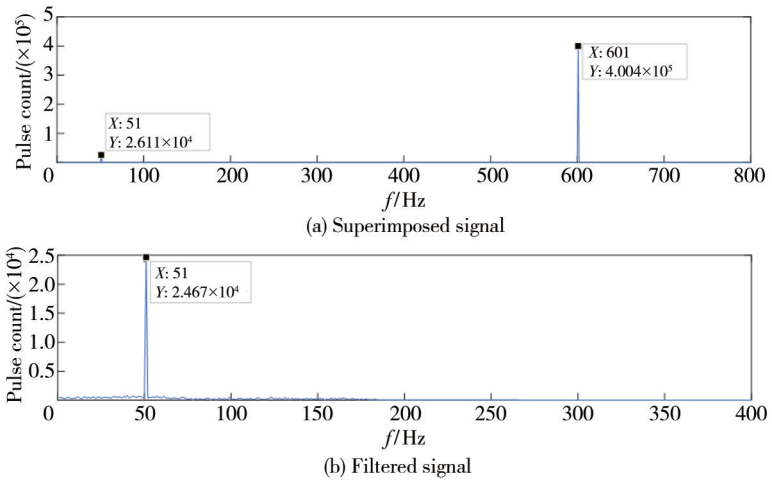

Fig. 12 Spectral analysis of gyro acquisition signal and filtered signal

The Verilog language was utilized in the FPGA integrated development environment (IDE) tool to write the filter module and accomplish IP call and configuration. The sampling frequency of the FIR IP core was set at 10 kHz, with an input data bit width of 16 bits. The output data bit width remains at 16 bits. At the same time, the generated test data file was stored in random access memory (RAM), with a data frequency matching the external gyro signal acquisition frequency of 4 kHz. After writing the code, Modelsim was utilized for conducting simulation tests.

The simulation results are presented in Fig. 13. In this figure, the data are depicted as an analog signal, where s_axis_data_tdata represents the input signal of the filter module and m_axis_data_tdata signifies the output signal of the filter module. Partial amplification of both input and output waveforms can be observed in Fig. 14. Frequency measurements were conducted using cursors, revealing an input signal frequency of 606.050 Hz and an output signal frequency rate of 53.050 Hz, thus confirming the successful implementation of filtering functionality.

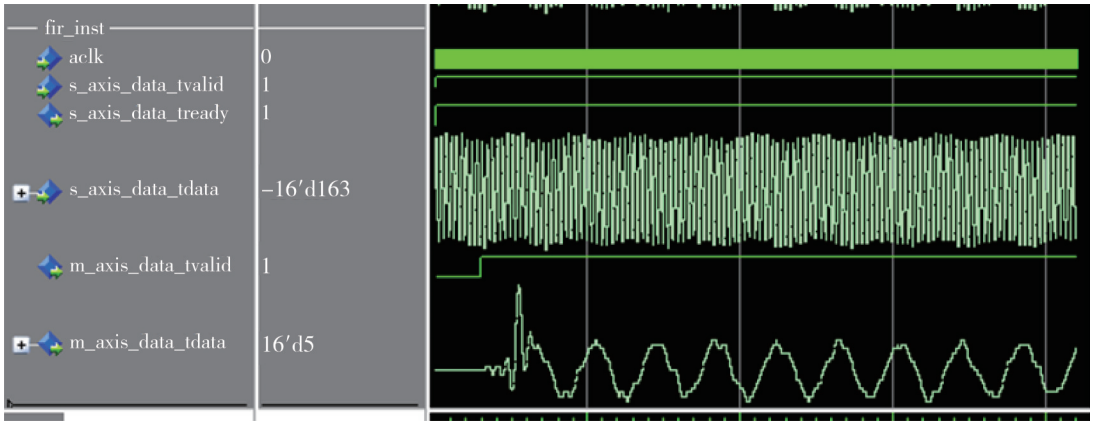

Fig. 13 Simulation diagram of filtering module

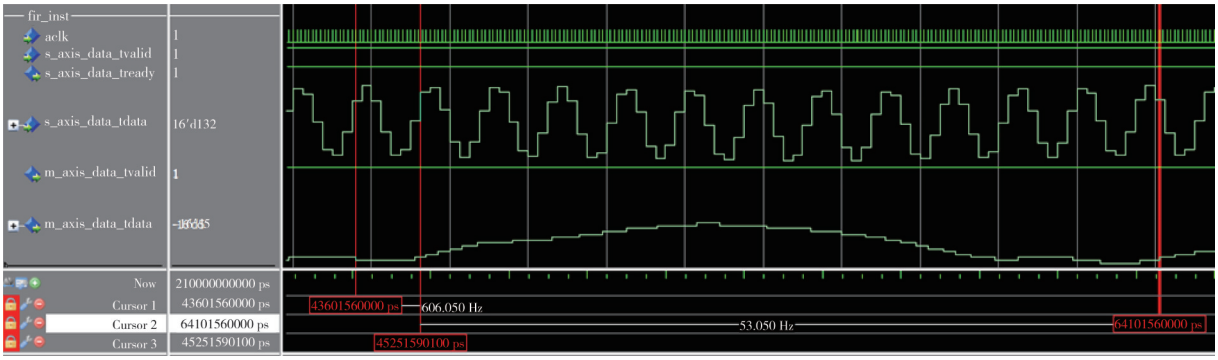

Fig. 14 Localized amplification of simulation waveform for the filtering module

3 Accelerometer signal acquisition

The inertial accelerometer is an instrument employed to measure the linear acceleration of a moving carrier. The quartz flexible accelerometer is one of its types, which utilizes Newton's second law for the detection of linear acceleration. Its principal components encompass the shell, quartz flexible support, torque coil, capacitive displacement sensor, magnetic steel, and mass block. The mass block detects linear acceleration along its sensitive axis, while the quartz flexible support offers support and adjustment functionalities. The quartz flexible accelerometer is capable of converting the acceleration information of the carrier into a current proportional to the acceleration via the internal circuit. By measuring the output current of the accelerometer, the magnitude of the acceleration can be obtained intuitively[24]. The quartz flexible accelerometer is a precision instrument featuring high precision, high sensitivity, low power consumption, excellent thermal stability, and ease of miniaturization. These characteristics render it widely utilized in industrial and scientific fields to meet the diverse requirements for the accurate measurement of acceleration physical quantities. This design utilizes the ZH1003 high-precision quartz flexural accelerometer , with detailed parameters listed in Table 1.

This design incorporates an accelerometer acquisition circuit to convert current signals into pulse signals, thereby

improving signal robustness against interference. The count of the converted pulse signals is utilized for deducing acceleration transformation. Each accelerometer, positioned on the carrier's X, Y, and Z axes, generates positive and negative pulse signals. A reversible counter with a 16-bit data bit width is employed for reversible counting the converted pulse signals. Taking the example of counting the output pulse signal from X-axis accelerometer on the carrier, Fig. 15 illustrates the implementation process of the accelerometer signal acquisition module. The reversible counter operates based on the logic level in the status register, performing addition and subtraction. It increments the counting value upon detecting the rising edge of a positive pulse signal and decrements it when a negative pulse signal's rising edge is detected. The module's sampling clock frequency is 4 kHz, aligning with the gyro's signal acquisition frequency. The input pulse counting ACC_X_CNT is gathered and transmitted to the subsequent module for further processing.

Table 1 Main parameters of ZH1003 quartz flexural accelerometer

Parameters	Value
Range/g	±30
Bias/mg	⩽±3
Scale factor/(mA•g^{-1})	[0.9, 1.3]
Second order nonlinear coefficient/(μg•g^{-2})	⩽±20
Bias repeatability/μg	⩽10
Scale factor repeatability	⩽20×10^{-6}
Working temperature/℃	[−40, 80]

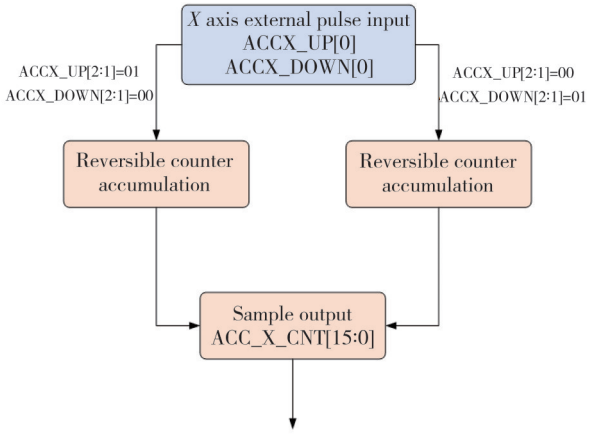

Fig. 15 Flow chart of accelerometer acquisition module

4 Data acquisition and analysis

4.1 Data acquisition and analysis of gyro

The system was positioned on the laboratory turntable for data testing and analysis. The turntable underwent continuous rotation along the X, Y, and Z axes at an angular rate of 10°/s. Subsequently, the collected data were transferred to the upper computer for storage over 10 min. A total of 4 000 data points were selected to generate waveform plots using Matlab software. The waveform display is shown in Fig. 16. The red line in the figure represents the real-time measured values of angular velocity for each axis, demonstrating the dynamic variation range of angular velocity at different sampling points.

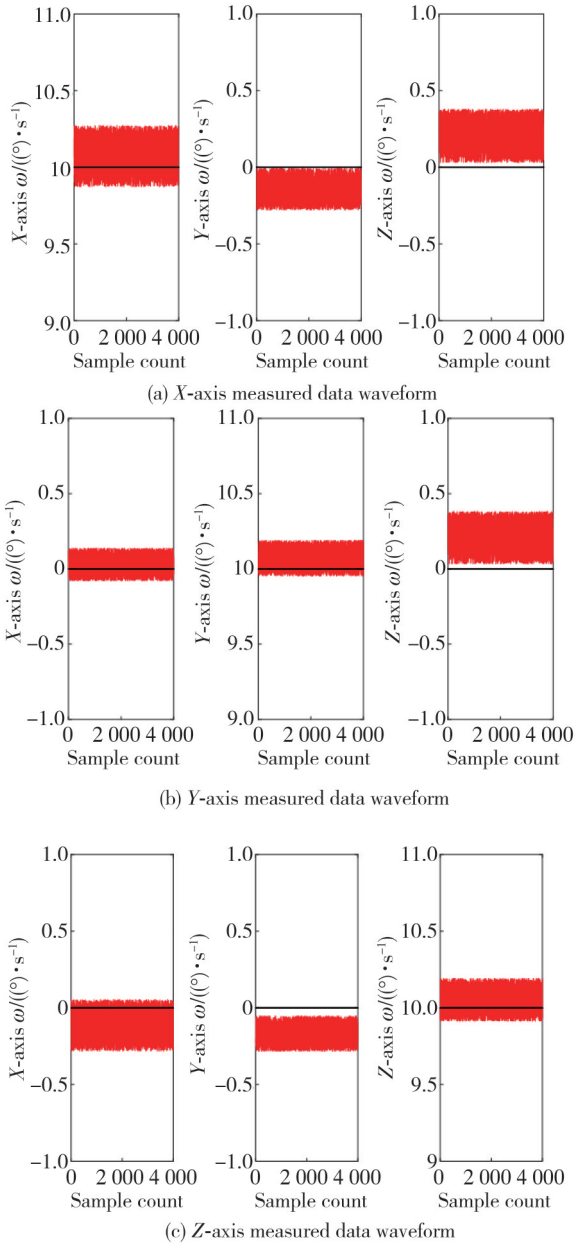

Fig. 16 Waveform of measurement data along X, Y and Z axes

Fig.16(a) illustrates the measured data waveform along the X axis. The gyro recorde an angular velocity of approximately 10° for this axis, while other axes show an angular velocity close to zero. Fig.16(b) and Fig.16(c) demonstrate that the test on angular velocity measurement using gyros across different axes yields normal results with successful data acquisition. This indicates that both the

hardware circuit based on platform and gyro signal acquisition module based on software program are operating normally.

The waveform can be utilized to assess the validity of collected data, followed by an analysis of the output data from the three-axis gyro to calculate mean values and root-mean-square errors. The results are listed in Table 2. It is evident that there exist certain inaccuracies in the measured data for each axis, which may arise due to circuit noise interference, installation deviations in laser gyros, uncalibrated calibration factors, and ambient temperature effects. These issues can be rectified by establishing a gyro error compensation model and conducting calibration procedures.

Table 2 Measurement data of gyro on *X*, *Y*, and *Z* axes

Axis	Set value/ $((^\circ)\cdot s^{-1})$	Mean error/ $((^\circ)\cdot s^{-1})$	Maximum error/ $((^\circ)\cdot s^{-1})$	Mean square error/$((^\circ)\cdot s^{-1})$
X-axis	10.000 0	0.048 9	0.249 8	0.115 0
Y-axis	10.000 0	0.070 3	0.188 0	0.068 5
Z-axis	10.000 0	0.040 0	0.178 0	0.080 6

4.2 Data acquisition and analysis of accelerometer

The design utilizes a quartz flexible accelerometer, known for its compact size and high impact resistance. The accelerometer was subjected to dynamic data testing in a centrifuge during the experiment, with a pulse signal acquisition period set at 100 ms. Multiple sets of data were collected and averaged to obtain the dynamic test results, as shown in Table 3.

Table 3 Dynamic measurement data of accelerometer

Acceleration/ $(m\cdot s^{-2})$	Output current/ mA	Sensitivity/ $(mA\cdot m^{-1}\cdot s^{2})$	Pulses count
−12	44.86	1.625	22 403
−8	38.36	1.628	19 156
−4	30.61	1.624	15 284
0	25.29	1.629	12 627
4	18.61	1.623	9 290
8	12.29	1.634	6 133
12	6.35	1.587	3 165

According to the output current and the number of pulses obtained, the fitting curve is analyzed to determine whether the pulse signal is collected correctly. The fitting curve of the current and pulse number is shown in Fig. 17. The formula of the generated fitting curve is $y=499.55x-6.790$. When the accelerometer current is converted to 1 mA, it generates 5 000 pulse signals per unit time, and the collection period in this design is 100 ms. Theoretically, the number of collected pulses should be 500. According to actual test data, the number of pulse signals collected in a single cycle can range from 500 ± 1, ensuring effective data collection with a pulse error within ±1.

The position of the accelerometers has been adjusted so that they are perpendicular to the horizontal plane on each axis. The waveform drawing is completed based on the measured data, as depicted in Fig. 18. The black line in the figure represents the theoretical measurement value of 1 g, and the measurement data error range for each axis accelerometer is within ±0.03 g, enabling effective acquisition of accelerometer data. Some reasonable deviations exist in the data, which can be corrected through error compensation in the future.

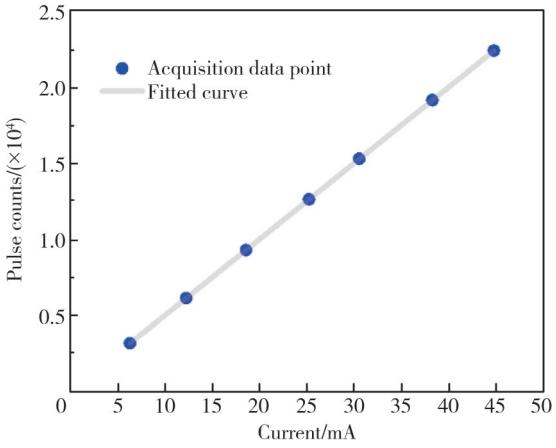

Fig. 17 Fitting curve of current and pulse counts

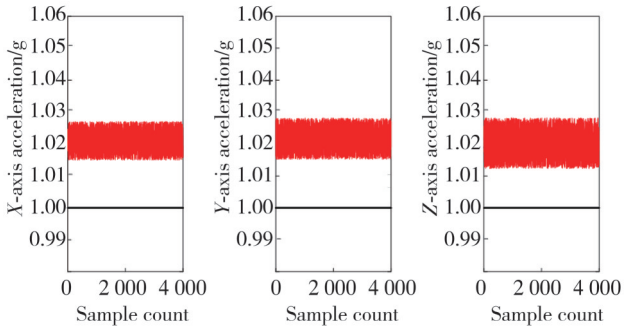

Fig. 18 Measurement of accelerometer data on *X*, *Y*, and *Z* axes

5 Conclusions

This paper presents the design of a signal acquisition circuit based on FPGA, leveraging an in-depth analysis of laser gyro and accelerometer output signals. The core processor XC7K325T-1 FFG900I is employed alongside domestic devices to achieve phase discrimination and frequency doubling of the gyro signal, while an FIR filter is utilized for gyro signal filtering. Furthermore, a quartz flexible accelerometer is used to collect the accelerometer signal through a reversible counter. The test results demonstrate errors within an acceptable range in the *X*, *Y*, and *Z* axes. The use of FPGA enhances configuration flexibility without

compromising filtering effectiveness as design requirements. Future research directions may involve establishing a more comprehensive gyro error compensation model and correcting errors through accurate calibration methods to improve the accuracy and stability of laser gyro systems, thereby advancing laser gyro applications.

Acknowledgement

We would like to express our sincere gratitude to the reviewers.

Declaration of conflicting interests

The authors have no conflict of interests related to this publication.

References

[1] CHOW W W, GEA-BANACLOCHE J, PEDROTTI L M, et al. The ring laser gyro. Reviews of Modern Physics, 1985, 57(1): 61-104.

[2] PESHEKHONOV V G. Gyroscopic navigation systems: Current status and prospects. Gyroscopy and Navigation, 2011, 2(3): 111-118.

[3] ZHAO Y C, CHENG J H, ZHAO L. Development status and future prospect of gyroscope in inertial navigation. Navigation and Control, 2019, 19(s1): 189-196.

[4] ZENG W. Research on laser gyro adaptive algorithm and FPGA implementation. Guizhou: Guizhou University, 2022.

[5] LI Y, FU L, WANG L L, et al. Laser gyro temperature error compensation method based on NARX neural network embedded into extended Kalman filter//YAN L, DUAN H, YU X, et al. Advances in Guidance, Navigation and Control. Singapore: Springer Singapore, 2021: 3309-3320.

[6] LIANG X J, JI H X. Mechanical vibration suppression technology of laser gyroscope based on variance analysis. Machinery Design & Manufacture, 2022(5): 88-91.

[7] JI H T, MAO Y H, CHEN D B, et al. Fundamental principle, current status and prospect of ring laser gyroscope. Navigation and Control, 2022, 21(5): 221-240.

[8] YU H Y, GAO CN, WANG S L, et al. Research on the development direction and dynamics of optical gyro// Dynamic Development Direction of Inertial Technology Integration and Application of Frontier Technology and Inertial Technology, October 19, 2021, Dalian, China. Beijing: Chinese Society of Inertial Technology, 2021: 11.

[9] DU F. Research on design and alignment technology of land strapdown inertial navigation computer. Harbin: Harbin Engineering University, 2020.

[10] LIAO K, YANG J Z, JU L, et al. Implementation of a capacitive digital isolator based on OOK modulation. Microelectronics & Computer, 2022, 39(9): 125-132.

[11] FENG X L, DENG M Y, HE S F, et al. A self-zeroing V/F-F/V signal isolation transmission circuit. Experimental Technology and Management, 2023, 40(7): 79-85.

[12] LIN Y, YIN W W, HU G M. Design and implementation of an automatic measuring device for nonlinear parameters of vibrating beam accelerometer. Computer Measurement & Control, 2023, 31(3): 119-126.

[13] ZHU J X, WANG W F, HUANG S P, et al. An improved calibration technique for MEMS accelerometer-based inclinometers. Sensors, 2020, 20(2): 452.

[14] ZHANG Z H, LI J M. Comparative study of A/D and I/F data acquisition system based on quartz flexible accelerometer. Computer Measurement & Control, 2021, 29(5): 179-183.

[15] ZHOU Z K. Research on signal processing technology of high-precision low-frequency quartz flexure accelerometer. Harbin: Harbin Institute of Technology, 2018.

[16] TANG H. Design and implementation of accelerometer I/F converter for strapdown inertial navigation system. Chongqing: Chongqing University of Technology, 2022.

[17] FAN Z F, LUO H, HU S M, et al. Angle random walk improvement analysis of body-dithered ring laser gyro based on lock-in error compensation. Infrared and Laser Engineering, 2023, 52(11): 3788.

[18] SUN W Q, CUI F Y, LIU J C, et al. System-level estimation and compensation of laser gyroscope sensitive axis dynamic offset. Chinese Journal of Inertial Technology, 2023, 31(7): 637-641.

[19] XIAO Z S, ZHANG H, ZHOU Y, et al. Research and development of resonant integrated optical gyroscope. China Laser, 2022, 49(19): 162-175.

[20] LI D, YU X D, WEI G, et al. Development status and trend of long-endurance laser gyro inertial navigation system. Journal of Optics, 2023, 43(17): 112-126.

[21] SHI Y F. Design of multi-channel data acquisition system based on PCI. Hangzhou: Zhejiang University, 2022.
MA Z G. Design of multi-channel data acquisition system based on PXI bus. Electronic Design Engineering, 2006.

[22] WANG Y, JIN L, ZENG F H. Design of multifunctional FIR digital filter based on FPGA. Modern Electronics Technique, 2023, 46(18): 38-42.

[23] SONG Z D, WANG Z G, LI J R, et al. Design and implementation of FIR digital filter based on FPGA. LCD & Display, 2020, 35(10): 1073-1078.

[24] ZHANG Z P. Design of large range precision I/F chip based on CMOS. Guiyang: Guizhou University, 2023.

基于FPGA的激光陀螺信号采集电路设计

陈 静, 李锦明*

中北大学 半导体与物理学院, 山西 太原 030051

摘 要: 随着电子技术的不断发展, 现场可编程门阵列(Field-programmable gate array, FPGA)在信号采集和处理领域展现出显著优势, 而信号采集是激光陀螺在实际应用中扮演的重要角色。通过深入分析激光陀螺和加速度计的输出信号, 设计了一种基于全国产化器件实现的激光陀螺信号采集电路, 使用有限脉冲响应(Finite impulse response, FIR)滤波器对陀螺信号滤波处理并采用体积小、抗冲击能力良好的石英挠性加速度计。仿真测试表明, X, Y, Z轴误差均在可接受范围且滤波效果符合设计要求。采用性能卓越的FPGA来完成信号的采集和预处理, 提高了配置的灵活性, 为激光陀螺应用系统的性能优化和信号处理提供了新的思路和方法。

关键词: 激光陀螺; 信号采集; 现场可编程门阵列; 有限脉冲响应滤波器; 加速度计

引用格式: CHEN Jing, LI Jinming. FPGA-based design of laser gyro signal acquisition circuit. Journal of Measurement Science and Instrumentation, 2025, 16(1): 107-118. DOI: 10.62756/jmsi.1674-8042.2025011